

Identification and Relative Quantification of Tyrosine Nitration in a Model Peptide Using Two-Dimensional Infrared Spectroscopy

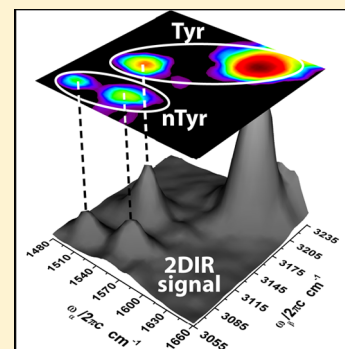
Lays Rezende Valim,[†] Julia A. Davies,[†] Karina Tveen Jensen,[‡] Rui Guo,^{†,§} Keith R. Willison,[†] Corinne M. Spickett,[‡] Andrew R. Pitt,[‡] and David R. Klug^{*,†}

[†]Department of Chemistry, Imperial College London, London SW7 2AZ, U.K.

[‡]School of Life and Health Sciences, Aston University, Aston Triangle, Birmingham B4 7ET, U.K.

S Supporting Information

ABSTRACT: Nitration of tyrosine in proteins and peptides is a post-translational modification that occurs under conditions of oxidative stress. It is implicated in a variety of medical conditions, including neurodegenerative and cardiovascular diseases. However, monitoring tyrosine nitration and understanding its role in modifying biological function remains a major challenge. In this work, we investigate the use of electron-vibration-vibration (EVV) two-dimensional infrared (2DIR) spectroscopy for the study of tyrosine nitration in model peptides. We demonstrate the ability of EVV 2DIR spectroscopy to differentiate between the neutral and deprotonated states of 3-nitrotyrosine, and we characterize their spectral signatures using information obtained from quantum chemistry calculations and simulated EVV 2DIR spectra. To test the sensitivity of the technique, we use mixed-peptide samples containing various levels of tyrosine nitration, and we use mass spectrometry to independently verify the level of nitration. We conclude that EVV 2DIR spectroscopy is able to provide detailed spectroscopic information on peptide side-chain modifications and to detect nitration levels down to 1%. We further propose that lower nitration levels could be detected by introducing a resonant Raman probe step to increase the detection sensitivity of EVV 2DIR spectroscopy.



1. INTRODUCTION

Oxidative damage of proteins is involved in mechanisms such as insulin resistance, cell-cycle arrest, senescence, and apoptosis.¹ Reactive oxygen/nitrogen species (ROS/RNS) such as the superoxide radical (O_2^-) and nitric oxide (NO) can be converted to peroxynitrite ($ONOOH/ONOO^-$),² which is a very strong oxidant. The principal targets of peroxynitrite in proteins are sulfhydryl and tyrosyl side chains with nitration of tyrosine (Tyr) to 3-nitrotyrosine (nTyr) being one of the most extensively studied ROS/RNS-driven post-translational modifications (PTMs).^{3–5}

Protein tyrosine nitration is thought to interfere with a range of biochemical processes⁶ and is known to prevent PTMs such as phosphorylation.^{5,7} Accumulation of nTyr is seen in neurodegenerative diseases,^{8–10} such as amyotrophic lateral sclerosis (ALS), Alzheimer's disease, and Parkinson's disease, as well as in chronic inflammation⁵ and cardiovascular disease.^{11,12} Conversely, at low NO concentrations, nitration of a specific Tyr residue (Tyr327) has been shown to have a positive regulatory effect through the activation of p53,¹³ a tumor-suppressant protein that acts as a transcription factor for various proteins involved in apoptosis and cell cycle arrest.

The main techniques currently employed for quantitative analysis of nTyr are immunoassays and mass spectrometry (MS) coupled to separation techniques, such as two-dimensional electrophoresis and liquid chromatography.^{1,5,14} Also, MS may be used in conjunction with chemical-labeling techniques to achieve higher selectivity and sensitivity.¹⁵

However, MS is a destructive technique that consumes the sample, and it relies on an interpretation of the patterns of ions generated upon fragmentation of the peptide, which can lead to false-positive identifications. Immunoassays depend highly on the quality of the antibodies involved and may suffer from selectivity issues.¹

The use of infrared spectroscopy to study proteins is beneficial because it relies on a sample's intrinsic vibrational properties, which allow for label-free and nondestructive analysis. However, backbone vibrational modes of proteins lead to very congested one-dimensional IR spectra. Thus, we turn to electron-vibration-vibration (EVV) two-dimensional infrared (2DIR) spectroscopy, a two-dimensional frequency domain technique, which is capable of probing both infrared and Raman transitions.^{16,17} When compared to one-dimensional IR spectroscopy, considerable spectral decongestion is achieved through EVV 2DIR spectroscopy due to its ability to spread information across two dimensions and to probe only coupled vibrational modes. These features make it a valuable technique in the study of complex systems such as proteins.

EVV 2DIR spectroscopy uses one visible/near-IR and two mid-IR picosecond laser beams to induce a nonlinear third-order process in the sample. When the variable mid-IR frequencies are resonant with coupled vibrational modes, a

Received: September 7, 2014

Revised: October 24, 2014

Published: October 27, 2014

four-wave mixing (FWM) process results, and the emitted photons are detected via a homodyne scheme, which leads to signal intensities proportional to the square of the number of molecules. The picosecond laser pulse durations are shorter than the vibrational coherence dephasing times, allowing the pulse ordering to be used with variable delays to select specific coherence pathways. By choosing the pulse ordering to follow $\omega_\alpha \rightarrow \omega_\beta \rightarrow \omega_\gamma$, we are able to select the nonparametric EVV-IR pathway (Figure 1).¹⁷ The ω_α pulse is required to be resonant with an IR-active vibrational mode, **a**, whereas ω_β must be resonant with an IR-active combination band **c**, which is equal to **a** + **b** (or an overtone) where **b** is a Raman-active mode. The Raman probe step, which is initiated by ω_γ , means that the FWM signal is dependent not only on the vibrational levels of the molecules studied but also on their electronic levels.

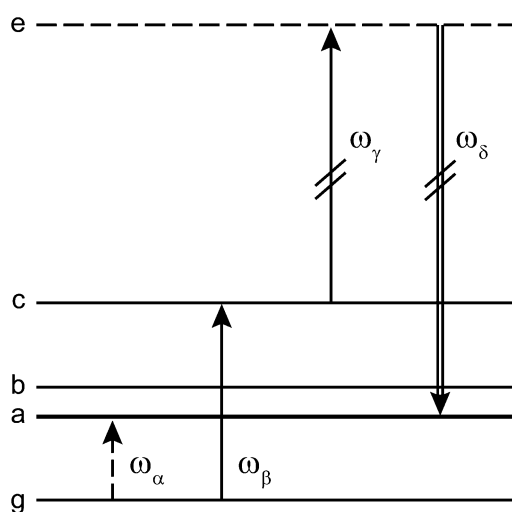


Figure 1. Schematic of an energy level diagram for the EVV-IR pathway depicting the generation of a signal beam through four-wave mixing of the ω_α , ω_β , and ω_γ laser beams. The time delay between successive laser pulses is typically chosen to be on the order of a few ps. The labels **a**, **b**, and **c** represent vibrational states, whereas **g** and **e** indicate the ground state and a virtual electronic state, respectively.

The results shown in this paper follow a doubly resonant setup, where the IR beams are in resonance with coupled vibrational modes of the molecule, whereas the ω_γ beam is scattered from a nonresonant (virtual) electronic level. However, it is possible for EVV 2DIR spectroscopy to be used as a triply resonant technique, where an electronic resonance is excited by the ω_γ beam. This resonant Raman enhancement is known to increase the signal by several orders of magnitude¹⁸ and can greatly improve the detection of vibrational modes coming from low-abundance species in complex samples.

In this paper, we report on the ability of EVV 2DIR spectroscopy to identify tyrosine nitration in model peptides, to quantify nitration levels in peptide mixtures down to 1%, and to differentiate between nTyr residues containing a neutral versus deprotonated hydroxyl group. This proof of concept lays the groundwork for the application of EVV 2DIR spectroscopy to the study of protein tyrosine nitration in complex samples through future implementation of a triply enhanced setup.

2. METHODS

2.1. Peptide Sample Preparation. Lyophilized powders of Ac-SPSYSPS-NH₂ and its nitrated version Ac-SPSnYSPS-NH₂ (Peptide Protein Research Ltd.) with greater than 98% purity were stored at -20 °C and allowed to thaw for 1 h before being dissolved in Milli-Q water to achieve a 10 mM concentration. NaOH solutions were used to adjust the pH to 5.6 and 9.1, which was measured using a double junction pH probe. For EVV 2DIR experiments, 1 μ L droplets for each peptide solution were deposited onto glass coverslips and dried under ambient conditions to form gel-phase coffee-ring structures that allow the peptides to remain hydrated.¹⁹ The height of each coffee ring is ~ 4 μ m, which was measured using a stylus profiler. On the basis of a shift in frequency of the electronic transition of nTyr upon deprotonation, the pH of the solution can be monitored throughout the drying process (neutral nTyr leads to bright yellow solution whereas its charged counterpart is dark orange). Because the dried spots remained the same color as their initial solutions, we can confirm that they retained their protonation state.

2.2. EVV 2DIR Spectroscopy. The experimental setup of EVV 2DIR spectroscopy has been described in detail elsewhere.²⁰ In brief, an ultrafast Ti:sapphire laser system (Newport Spectra-Physics) is used to generate a near-IR laser beam at 790 nm with a pulse duration of 1 ps and a repetition rate of 1 kHz. The generated beam is split into three beams, two of which are directed toward optical parametric amplifiers (Newport Spectra-Physics) to generate 1 ps pulses with tunable mid-IR frequencies calibrated using a 38 μ m thick polystyrene calibration film traceable to NIST 1921b frequencies. All three beams are linearly polarized parallel to the plane of propagation (PPP), spatially overlapped, and focused at the sample. The pulse energy of the near-IR beam is set to 200 nJ at the sample, and the mid-IR beams display near-symmetric energy profiles across an $\omega_\alpha/2\pi c$ range from 1300 to 1700 cm^{-1} ($E_{\text{max}} = 800$ nJ at 1500 cm^{-1}) and an $\omega_\beta/2\pi c$ range from 2600 to 3400 cm^{-1} ($E_{\text{max}} = 2.0$ μ J at 3000 cm^{-1}). These pulse energies are measured through a 100 μ m diameter pinhole because it closely matches the $1/e^2$ diameter of the near-IR beam, which defines the sample area from which the FWM signal is generated. Delay stages are used to adjust the variable delays between the laser pulses, thus controlling their arrival times to the order $\omega_\alpha \rightarrow \omega_\beta \rightarrow \omega_\gamma$, which leads to the coherence pathway described in Figure 1. The emitted signal is monitored using a photomultiplier detector (Hamamatsu H7422-50).

Prior to measuring spectra, the system is enclosed and purged with N₂ to reduce the humidity level to less than 3%. Unless otherwise stated, EVV 2DIR spectra were obtained using pulse time delays of $\tau_{\alpha\beta} = 1.75$ ps and $\tau_{\beta\gamma} = 1$ ps, a mid-IR frequency step size of 5 cm^{-1} , and an acquisition rate of 100 laser shots per data point. The FWM signal intensity was normalized to the methylene cross-peak at 1465/2925 cm^{-1} and smoothed using the shrinking/expanding algorithm in OriginPro (OriginLab Co.). The data were then plotted as a contour map with a logarithmic scale.

2.3. DFT Calculations and EVV 2DIR Simulations. As previously described,²¹ GAUSSIAN 03 is used to perform DFT calculations at B3LYP/6-311++G(p,d) level of theory, and a scaling factor of 0.98 is applied to the resulting vibrational frequencies. The theoretical EVV 2DIR signal intensity corresponding to the pathway shown in Figure 1 was numerically calculated as a function of the IR frequencies

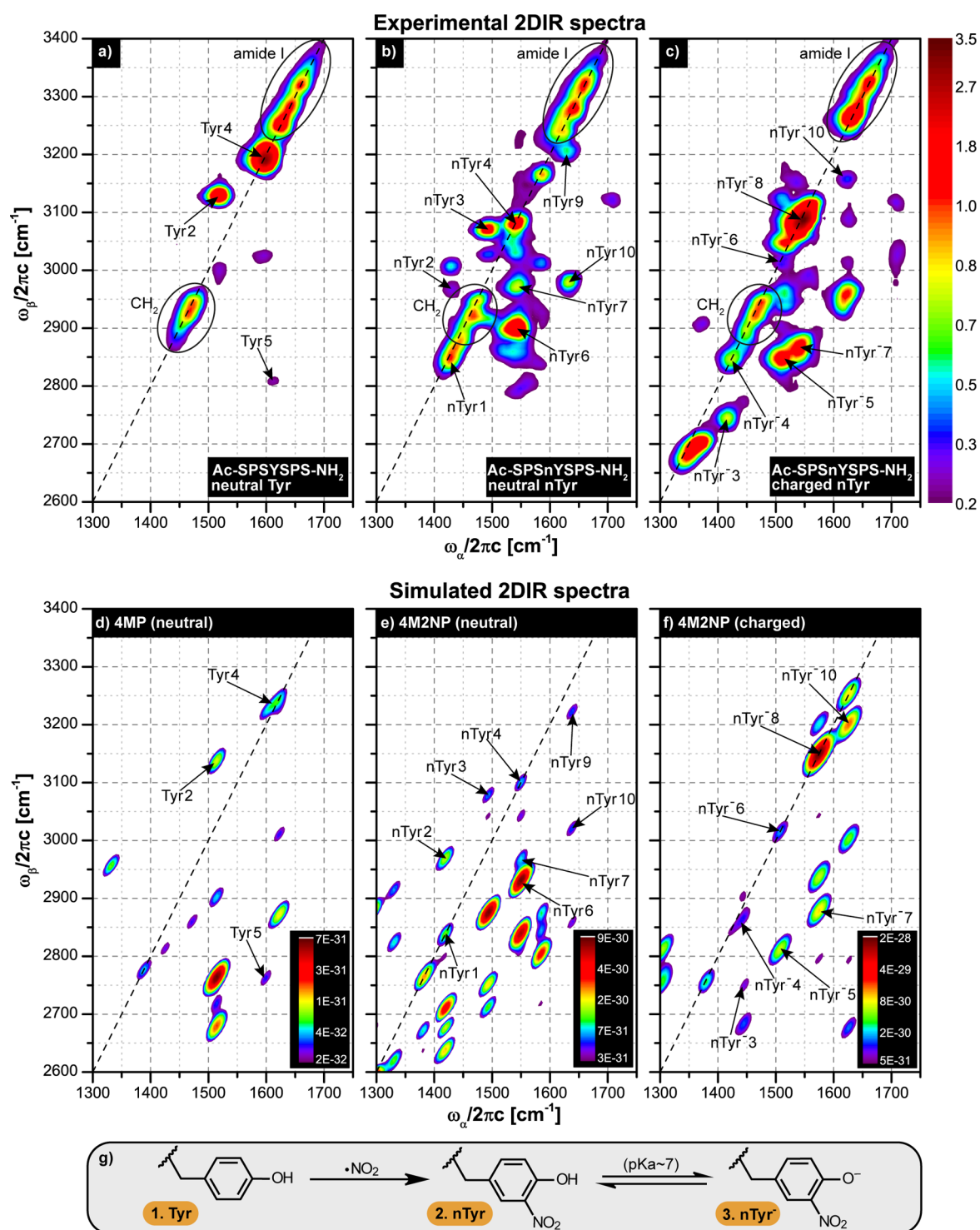


Figure 2. Experimental EVV 2DIR spectra for (a) Tyr heptamer at pH 9.1, (b) nTyr heptamer at pH 5.6, and (c) nTyr heptamer at pH 9.1. The CH₂ and amide I cross-peaks are circled and are common to all three spectra. Simulated EVV 2DIR spectra for (d) neutral 4-methylphenol (4MP), (e) neutral 4-methyl-2-nitrophenol (4M2NP), and (f) deprotonated 4M2NP, where 4MP and 4M2NP are side-chain analogues of Tyr and nTyr, respectively. Correlations between cross-peaks observed in the experimental and simulated spectra for Tyr or nTyr are indicated by labels and arrows, whereas the diagonal dashed lines highlight cross-peaks arising from couplings between fundamental modes and their overtones. (g) Scheme of compounds illustrating Tyr nitration via reaction with the nitrogen dioxide radical and deprotonation of the nTyr hydroxyl group.

employing the method reported by Kwak et al.²² The resulting simulated EVV 2DIR spectra were produced by representing each cross-peak as a 2D Gaussian function with a full width at half maximum (fwhm) of 20 cm⁻¹ and a center frequency matching the harmonic frequencies of the bands involved.

2.4. Liquid Chromatography-Mass Spectrometry. The peptide mixtures were diluted to 4 μM and separated on an Ultimate 3000 liquid chromatography system (Dionex, Camberley, U.K.) interfaced with a 5600 TripleTOF mass spectrometer (ABSciex, Warrington, U.K.) via a New Objective

PicoTip emitter (FS360-20-10-N, Woburn, MA, USA) controlled by Chromeleon Xpress and Analyst software (TF v1.5, ABSciex). The peptides were captured and desalted on a C18RP precolumn (C18 PepMapTM, 5 μm , 5 mm \times 0.3 mm i.d., Dionex, Bellefonte, PA, USA) by washing for 4 min with 2% aqueous acetonitrile (0.1% formic acid) at 30 $\mu\text{L}/\text{min}$. The peptides were then separated on a C18 nano-HPLC column (C18 PepMapTM, 5 μm , 75 μm i.d. \times 150 mm, Dionex) using a gradient elution running from 2 to 45% aqueous acetonitrile (0.1% formic acid) in 60 min and a final washing step running from 45 to 90% aqueous acetonitrile (0.1% formic acid) in 1 min. The system was then washed with 90% aqueous acetonitrile (0.1% formic acid) for 5 min and equilibrated with 2% aqueous acetonitrile (0.1% formic acid).

Mass spectrometer settings were as follows: spray voltage, 2.4 kV; source temperature, 150 $^{\circ}\text{C}$; declustering potential, 50 V; and curtain gas, 15. Survey TOF MS scans were collected in high-resolution positive ion mode from 350 to 1250 Da for 500 ms. MS/MS data were collected using information-dependent acquisition (IDA) with the following criteria: the three most intense ions with 1+ to 3+ charge states and a minimum intensity of 200 counts per second (cps) were chosen for analysis using dynamic exclusion for 10 s, a 500 ms acquisition time, and rolling collision energy.

Raw data were analyzed with PeakView (ABSciex). Accurately prepared solutions were used to measure the relative signal intensities of the two peptides using the sum of the corresponding extracted ion chromatograms (XICs), of the Gaussian smoothed by 4 points, of the 1+ and 2+ charge states, and of the protonated and monosodium adduct of both charge states. The nTyr-containing peptide signals were calculated to be approximately 2.61 times more intense than those of the native peptide; this factor was used to correct the data for the mixed peptides.

3. RESULTS AND DISCUSSION

3.1. Experimental EVV 2DIR Spectra. EVV 2DIR spectra have been measured for two similar heptamer peptides, one of which contains a single Tyr residue (Ac-SPSYSPS-NH₂) and the other a single nTyr residue (Ac-SPSnYSPS-NH₂); the resulting spectra are presented in Figure 2a–c. A scheme of the compounds is also provided in Figure 2g to illustrate the mechanism of Tyr nitration to nTyr and deprotonation of the nTyr hydroxyl group. Because the $\text{p}K_{\text{a}}$ of the hydroxyl group in Tyr decreases from ~ 10 to ~ 7 upon nitration,²³ nTyr species containing the neutral and deprotonated hydroxyl are expected to be present in an approximately 1:1 ratio at physiological pH. Therefore, to obtain the spectral signal for nTyr in each of the two protonation states, spectra have been recorded at pH values greater than 1 pH unit away from the nTyr $\text{p}K_{\text{a}}$. A clear difference between the nTyr spectral signatures at pH 5.6 and 9.1 is observed in Figure 2b and c.

In general, the experimental EVV 2DIR spectra measured for the two protonation states of the nTyr peptide display a number of cross-peaks larger than that for the unmodified Tyr peptide; however, there are also several similarities between the spectra, and these will be discussed first. The cross-peak with components at 1460/2920 and 1470/2940 cm^{-1} is observed for all three spectra shown in Figure 2a–c and can be assigned to a CH₂ scissor vibration, where the $\omega_{\alpha}/2\pi\text{c}$ and $\omega_{\beta}/2\pi\text{c}$ frequency values correspond to the fundamental mode and the overtone band, respectively. The observed structure in the cross-peak is discussed in detail elsewhere.²⁴ Each heptamer contains a total

of 11 CH₂ groups: one for each Ser residue, three for each Pro residue, and one for each Tyr or nTyr residue. In previous work by our group, ratios of the side-chain cross-peak intensities with respect to an internal reference were determined in which the internal reference was either the CH₂²⁵ or CH₃²⁶ cross-peak intensity. Because the peptides used in the present work contain only a single CH₃ group, which is in the acetyl group of the N-terminal end cap, the CH₂ cross-peak intensity is used as the internal reference here.

The elongated diagonal feature centered at $\sim 1640/3280$ cm^{-1} is present in the spectra of all three peptides (circled in Figure 2a–c) and can be assigned to the amide I band fundamental and its overtone. This band is predominantly associated with the backbone C=O stretch mode, rendering it sensitive to the peptide's secondary structure and its environment. The amide I band has been extensively studied using conventional 2DIR spectroscopic techniques to obtain information on the conformation and aggregation of peptides and proteins. However, in the present work, the experimental conditions have been optimized to directly probe vibrational modes associated with the Tyr and nTyr side chains rather than the amide I band. This has resulted in an optical density of ~ 1 for the amide I band, which is too high for detailed analysis and interpretation of the band structure; thus, only a basic discussion of the substructure will be provided here. In Figure 2a–c, component peaks are observed at approximately 1620/3240, 1635/3270, and 1660/3320 cm^{-1} , which arise from structural inhomogeneity in the sample. On the basis of extensive literature describing amide I substructures, we can assign the highest frequency component at 1660/3320 cm^{-1} to either a short α helix or a disordered structure, whereas the component that appears at $\sim 1635/3270$ cm^{-1} can be assigned to β strands.²⁷ The third component at 1620/3240 cm^{-1} is in close agreement with frequencies reported to arise from a red-shift of the β -strand component due to proline residues.²⁸ The relative intensities of these three frequency components vary dramatically among the spectra shown in Figure 2a–c, suggesting that the peptide conformation and/or aggregation changes upon tyrosine nitration and is also dependent on the protonation state. However, we refrain from drawing any further conclusions because of the high optical density for the amide I band, as discussed above.

A cross-peak at 1710/3120 cm^{-1} is observed in the spectra for the neutral and deprotonated states of the nTyr peptide (Figure 2b and c) and is assigned to the C=O stretch of the acetyl end cap on the N-terminus of each peptide. The deprotonated nTyr side chain also contains a C=O group; however, the quantum chemistry calculations discussed in section 3.2 and in the Supporting Information indicate that the frequency of this peak is much lower than 1710 cm^{-1} , possibly due to the negative charge that results from deprotonation. The intensity of the peak at 1710/3120 cm^{-1} is ~ 4 times weaker for the Tyr peptide and is not visible in Figure 2a due to the lower limit used for the intensity range, which has been chosen so that the strong features are more easily discernible. In our experience, the appearance of CH₂, amide I, and C=O stretch cross-peaks in EVV 2DIR spectra is typical for peptides and proteins.

The main differences between the spectra shown in Figure 2a–c are the presence or absence of cross-peaks associated with the side chains of Tyr (Figure 2a), neutral nTyr (Figure 2b), and deprotonated nTyr (Figure 2c). It is interesting to note that the spectral fingerprint is very different for each of the

Table 1. Comparison between Experimental and Simulated Cross-Peak Frequencies for Tyr and Their Vibrational Assignments

peak label	experimental frequency (cm ⁻¹)	simulated frequency (cm ⁻¹)	vibrational assignment ^a
Tyr1	1520/3000	1514/3028 ^b	CH rock (19a)/2[CH rock (19a)]
Tyr2	1520/3130	1514/3137	CH rock (19a)/CH rock (19a) + CC stretch (8a)
Tyr3	1595/3025	1623/3049 ^b	CC stretch (8a)/CC stretch (8a) + CC stretch (19b)
Tyr4	1600/3190	1623/3246	CC stretch (8a)/2[CC stretch (8a)]
Tyr5	1615/2810	1599/2762	CC stretch (8b)/CC stretch (8b) + COH bend

^aNumbers in parentheses are aromatic mode assignments in Varsanyi notation. ^bThis is a weak peak in the simulated spectrum.

Table 2. Comparison between Experimental and Simulated Cross-Peak Frequencies for Neutral nTyr and Their Vibrational Assignments

peak label	experimental frequency (cm ⁻¹)	simulated frequency (cm ⁻¹)	vibrational assignment ^a
nTyr1	1430/2850	1419/2838	CC stretch (19b)/2[CC stretch (19b)]
nTyr2	1430/2965	1419/2969	CC stretch (19b)/CC stretch (19b) + asymm NO ₂ stretch
nTyr3	1490/3070	1494/3078	CH rock (19a)/CH rock (19a) + CC stretch (8b)
nTyr4	1540/3080	1550/3100	asymm NO ₂ stretch/2[asymm NO ₂ stretch]
nTyr5	1545/2795	1550/2808 ^b	asymm NO ₂ stretch/asymm NO ₂ stretch + symm NO ₂ stretch
nTyr6	1545/2900	1550/2931	asymm NO ₂ stretch/asymm NO ₂ stretch + CC stretch (14)
nTyr7	1545/2970	1550/2969	asymm NO ₂ stretch/asymm NO ₂ stretch + CC stretch (19b)
nTyr8	1585/3165	1584/3168 ^b	CC stretch (8b)/2[CC stretch (8b)]
nTyr9	1630/3205	1638/3222	CC stretch (8a)/CC stretch (8a) + CC stretch (8b)
nTyr10	1635/2980	1638/3019	CC stretch (8a)/CC stretch (8a) + CC stretch (14)

^aNumbers in parentheses are aromatic mode assignments in Varsanyi notation. ^bThis is a weak peak in the simulated spectrum.

Table 3. Comparison between Experimental and Simulated Cross-Peak Frequencies for Deprotonated nTyr and Their Vibrational Assignments

peak label	experimental frequency (cm ⁻¹)	simulated frequency (cm ⁻¹)	vibrational assignment ^a
nTyr ⁻ 1	1365/2700 ^b	1361/2722 ^c	CH rock (3)/CH rock (3) + CC stretch (14)
nTyr ⁻ 2	1375/2910	1361/2936 ^c	CH rock (3)/CH rock (3) + CO stretch
nTyr ⁻ 3	1415/2745	1446/2750	asymm NO ₂ stretch/asymm NO ₂ stretch + CC stretch (14)
nTyr ⁻ 4	1420/2845	1446/2867	asymm NO ₂ stretch/asymm NO ₂ stretch + CH rock (19a)
nTyr ⁻ 5	1510/2845	1507/2811	CC stretch (8b)/CC stretch (8b) + CC stretch (14)
nTyr ⁻ 6	1510/3010	1507/3014	CC stretch (8b)/2[CC stretch (8b)]
nTyr ⁻ 7	1540/2865	1575/2879	CO stretch/CO stretch + CC stretch (14)
nTyr ⁻ 8	1545/3085	1575/3150	CO stretch/2[CO stretch]
nTyr ⁻ 9	1625/2965	1626/2930 ^c	CC stretch (8a)/CC stretch (8a) + CC stretch (14)
nTyr ⁻ 10	1625/3160	1626/3201	CC stretch (8a)/CC stretch (8a) + CO stretch

^aNumbers in parentheses are aromatic mode assignments in Varsanyi notation. ^bThis feature is broad and contains several unresolved peaks. ^cThis is a weak peak in the simulated spectrum.

three peptide samples. There are five obvious cross-peaks in Figure 2a that can be assigned to vibrational modes of the Tyr side chain. In order of decreasing intensity, the frequencies of these peaks are 1600/3190, 1520/3130, 1595/3025, 1520/3000, and 1615/2810 cm⁻¹. In previous work using EVV 2DIR spectroscopy, two Tyr cross-peaks were observed in the spectra of various peptides containing Tyr residues.^{25,26} A very weak peak was observed at 1470/3040 cm⁻¹, and a strong peak was observed at 1530/3130 cm⁻¹. The latter peak was assigned to $\nu_{13}/(\nu_{13} + \nu_{16})$, where ν_{13} is an aromatic stretching mode, and ν_{16} is a CH₂ deformation mode on the Tyr side chain. Assignments of the remaining cross-peaks for Tyr and nTyr residues will be based on DFT calculations and simulated EVV 2DIR spectra.

3.2. Spectral Characterization. For the purpose of characterizing the experimental EVV 2DIR spectra presented in Figure 2a–c, EVV 2DIR spectra have been simulated for 4MP and 4M2NP, and the results are presented in Figure 2d–f. These molecules are side-chain analogues of Tyr and nTyr residues. Each simulated spectrum is placed directly below the

corresponding experimental spectrum to aid comparison. The correlation between the relative intensities of the cross-peaks for each pair of spectra is not expected to be strong because the simulations do not consider the variable lifetimes of the coherences excited by the IR laser pulses. In addition, the incident laser intensity at the peptide sample varies with the tunable IR frequency for both the ω_{α} and ω_{β} beams. However, the frequencies of the cross-peaks are expected to agree to within 50 cm⁻¹ in most cases.

Before comparing the cross-peak frequencies between the simulated and experimental spectra in more detail, we first discuss the differences observed for the three simulated spectra only. In this case, we can compare the intensities because the method used to perform the simulations is the same for all three spectra. From Figure 2d–f, it is clear that the maximum signal intensity calculated for these side-chain analogues varies greatly; the signals from the deprotonated and neutral states of 4M2NP are 14 and 229 times higher, respectively, than that for neutral 4MP. In other words, the simulated spectra predict that the experimental signal intensity from nTyr residues will be

substantially higher than that from Tyr residues. Another observation from the simulated spectra is that there are substantially larger numbers of cross-peaks observed in both of the 4M2NP spectra than in the 4MP spectrum. The same observation is made in the experimental spectra (Figure 2a–c).

Tables 1, 2, and 3 list the assignments and vibrational frequencies for a selection of cross-peaks observed in the experimental EVV 2DIR spectra; there are five peaks for Tyr, ten peaks for neutral nTyr, and ten peaks for deprotonated nTyr, each of which is given a unique peak label for easy identification. Each cross-peak assignment consists of two parts; the first corresponds to the mode description for the fundamental band excited by the first mid-IR laser pulse, and the second gives an assignment for the combination band or overtone excited by the second mid-IR laser pulse. For aromatic modes, a descriptive assignment is given along with a numerical label in parentheses, which follows Varsanyi notation.²⁹ This notation has been chosen because it extends the Wilson³⁰ vibrational mode numbering system for benzene to cover more than 700 benzene derivatives, and it provides general rules for the assignment of additional benzene derivatives based on the anticipated frequency and vibrational motion of each mode, thus removing some of the ambiguity often associated with mode assignment using alternative schemes. Details of the assignments for the fundamental modes are given in the Supporting Information, along with a comparison of the calculated and experimental frequencies for each mode (Tables S1, S2, and S3).

The correlation between the cross-peaks in the experimental and simulated spectra is indicated by the peak labels shown in Figure 2 and Tables 1–3. For the Tyr peptide, three of the five cross-peaks observed in the experimental spectrum (Figure 2a) correlated with cross-peaks in the simulated spectrum (Figure 2d); these peaks are labeled Tyr2, Tyr4, and Tyr5. Upon initial inspection of the spectra, one might presume that the simulated cross-peak at 1623/3011 cm^{-1} correlates with the experimental cross-peak at 1595/3025 cm^{-1} (Tyr3). However, the simulated cross-peak, which is assigned to CC stretch (8a)/CC stretch (8a) + CH_3 umbrella, is an artifact because the side-chain analogue contains a CH_3 group that is not present in the Tyr residue. This is also true for the series of four simulated cross-peaks observed between 1388/2776 and 1514/2902 cm^{-1} in Figure 2d. The assignments for all five of the Tyr cross-peaks observed in the experimental spectrum are presented in Table 1.

A good understanding of the spectral signature for nTyr in both protonation states is indicated by the substantial number of cross-peaks that have been successfully correlated and assigned in Tables 2 and 3; these correlations are also indicated in Figure 2. For the protonated nTyr peptide, the two most intense cross-peaks observed in the experimental spectrum have frequencies of 1545/2900 and 1540/3080 cm^{-1} and are labeled nTyr6 and nTyr4, respectively, in Figure 2b and Table 2. The first component of these cross-peaks ($\sim 1545 \text{ cm}^{-1}$) is assigned to the asymmetric NO_2 stretch vibration, indicating that these spectral features can provide information relating to the site of the peptide modification. Three less intense cross-peaks at 1430/2965, 1545/2795, and 1545/2970 cm^{-1} (nTyr2, nTyr5, and nTyr7, respectively) also involve excitation of the asymmetric NO_2 stretch mode. In contrast, the cross-peaks at 1630/3205 and 1635/2980 cm^{-1} (nTyr9 and nTyr10, respectively) are associated with a CC stretch (8a) aromatic mode, which is the mode responsible for the most intense peak

in the unmodified Tyr peptide spectrum at 1600/3190 cm^{-1} (Tyr4 in Table 1 and Figure 2a).

In the experimental spectrum for the deprotonated nTyr peptide, there are two cross-peaks at 1415/2745 and 1420/2845 cm^{-1} that have fundamental frequencies assigned to the asymmetric NO_2 stretch mode, and these peaks are labeled nTyr⁻3 and nTyr⁻4, respectively, in Figure 2c and Table 3. However, the most intense cross-peak is at 1545/3085 cm^{-1} (nTyr⁻8) and is assigned to the fundamental and overtone of the CO stretch mode. As revealed in Table S3 in the Supporting Information, the CO stretch mode contains significant asymmetric NO_2 stretch motion as well as stretching motion along the CO bond. It is also interesting to note that half of the cross-peaks in Table 3 (nTyr⁻1, nTyr⁻3, nTyr⁻5, nTyr⁻7, and nTyr⁻9) have combination bands containing the CC stretch (14) mode, which can be explained by the very high Raman intensity calculated for this mode (Supporting Information). The detailed spectral characterization that we have achieved could potentially be used to interpret changes in EVV 2DIR spectra that result from an altered environment around nTyr residues when studied under complex biological conditions.

3.3. Experimental EVV 2DIR Spectra for Peptide Mixtures. To ascertain whether EVV 2DIR spectroscopy could be used to determine the percentage of tyrosine that is nitrated in a peptide or protein sample, it is first necessary to determine the relationship between the relative intensities of the Tyr and nTyr cross-peaks and the percentage of nitration. This characterization can be performed using samples containing known proportions of Tyr and nTyr residues; therefore, EVV 2DIR spectra have been measured for five different peptide mixtures containing 0, 25, 50, 75, and 100% of nTyr heptamer Ac-SPSnYSPS-NH₂, with the non-nitrated version constituting the remainder of the peptide mixture. The resulting spectra measured at pH 5.6 are presented in Figure 3a–e. The spectrum at 0% nTyr (Figure 3a) displays the spectral signature for Tyr residues and is similar to that shown in Figure 2a, which was measured for a Tyr peptide sample at pH 9.1. This similarity is expected because the Tyr side chain is neutral at both pHs. The 50% nTyr mixture contains equal amounts of the nTyr and Tyr peptides; therefore, this spectrum (Figure 3c) provides a simple indication of whether the signal is more intense from a Tyr or an nTyr residue. In this case, the Tyr peak at 1600/3190 cm^{-1} is the most intense. This contradicts the results from the simulations, which incorrectly predicted that the signal from neutral nTyr would be ~ 14 times higher than that from Tyr. This discrepancy is most likely due to inaccuracies in the quantum chemistry calculations caused by the use of a simplified molecular model that neglects the effects of hydrogen bonding due to water solvation and peptide interactions.

As discussed in section 1, a homodyne-detected signal is produced by a FWM process in EVV 2DIR experiments; therefore, the measured signal intensity is proportional to the square of the number of peptides that contribute to the signal. Thus, for the mixed-peptide samples at pH 5.6, the square root of the signal intensity has been plotted against the percentage of nTyr peptides for various Tyr and nTyr cross-peaks, and the results are shown in Figure 3f. As expected, the signal intensity of the Tyr cross-peak at 1600/3190 cm^{-1} (Tyr4) decreases as the percentage of nTyr peptide increases, whereas the nTyr cross-peaks at 1540/3080, 1545/2900, and 1635/2980 cm^{-1} (nTyr4, nTyr6, and nTyr10, respectively) show an increase in

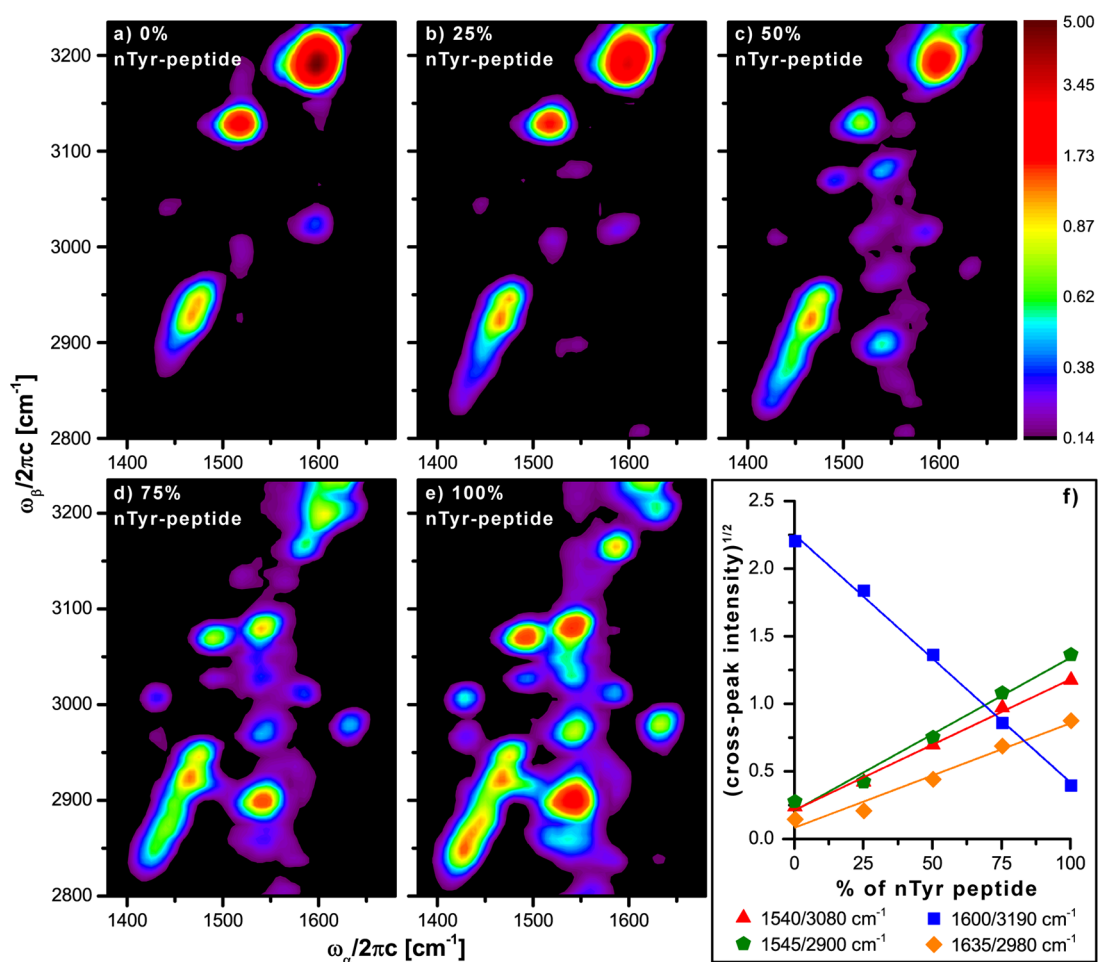


Figure 3. Experimental EVV 2DIR spectra for mixtures of the Tyr and nTyr heptamers at pH 5.6 containing (a) 0, (b) 25, (c) 50, (d) 75, and (e) 100% of the neutral nTyr peptide. The Tyr cross-peak intensities decrease and the nTyr cross-peak intensities increase with an increasing percentage of nTyr in the peptide mixture. (f) Given that the signal depends on the square of the number of molecules, the square root of the normalized cross-peak intensity is plotted against the percentage of nTyr peptide. The linear regressions provide calibration curves from which the percentage of nTyr in a sample can be determined from the normalized cross-peak intensity.

signal intensity. The solid lines represent linear regressions and indicate a good linear correlation between the square root of the signal intensity and the percentage of nTyr with R^2 values between 0.973 and 0.995. From these linear regressions, the ratio of intensities for a chosen nTyr peak with respect to a Tyr peak can be interpolated at any percentage of nTyr. This provides our calibration curve, such that the percentage of nitration in a wide variety of samples can be uniquely determined from a measurement of the relative intensities of a pair of nTyr and Tyr cross-peaks in the EVV 2DIR spectrum. In cases where the spectrum of a sample is particularly congested, measuring the relative intensities of more than two nTyr and Tyr peaks may be preferred.

For the 25% nTyr peptide mixture at pH 5.6 used in the present work, the EVV 2DIR spectrum (Figure 3b) reveals that two nTyr cross-peaks at 1540/2900 and 1540/3080 cm^{-1} are easily observable, indicating that the detection limit for tyrosine nitration is well below 25%. A more accurate estimation can be determined from the plot in Figure 3f by taking the difference between the y -value for a data point and the y -value predicted by the linear regression for a chosen nTyr cross-peak for both the 0 and 25% nTyr peptide mixtures. The sum of these differences, which indicates the uncertainty in the cross-peak intensities, is converted to a percent nTyr value using the slope

of the linear regression. An average value for all three nTyr peaks in Figure 3f provides a conservative estimate of $\sim 12\%$ as the detection threshold level for tyrosine nitration. Even though a sensitivity limit of $\sim 12\%$ may seem high, the potential for substantial improvement only requires using a resonant Raman probe step as mentioned in section 1. Furthermore, the advantage of this technique is that it does not require any background subtraction or deconvolution of the spectral features, making data analysis unambiguous and prompt.

Spectra measured for the peptide mixtures at pH 9.1 for the deprotonated state of nTyr are presented in Figure 4. The 50% nTyr spectrum (Figure 4c) reveals that the nTyr peak at 1545/3085 cm^{-1} (nTyr⁻⁸) is more intense than the Tyr peak at 1600/3190 cm^{-1} (Tyr⁴), indicating that the signal from deprotonated nTyr is stronger than that from non-nitrated Tyr. The relative intensities of the nTyr and Tyr cross-peaks in the 25% nTyr spectrum are significantly higher for the deprotonated sample (Figure 4b) than for the neutral sample (Figure 3b); therefore, the detection sensitivity for Tyr nitration is expected to be higher for the deprotonated nTyr sample also. Furthermore, the measured R^2 values of greater than 0.984 for all four of the nTyr cross-peaks (nTyr⁻¹, nTyr⁻², nTyr⁻⁸, and nTyr⁻⁹) indicate good linear correlation between the square root of the signal intensity and the percentage of

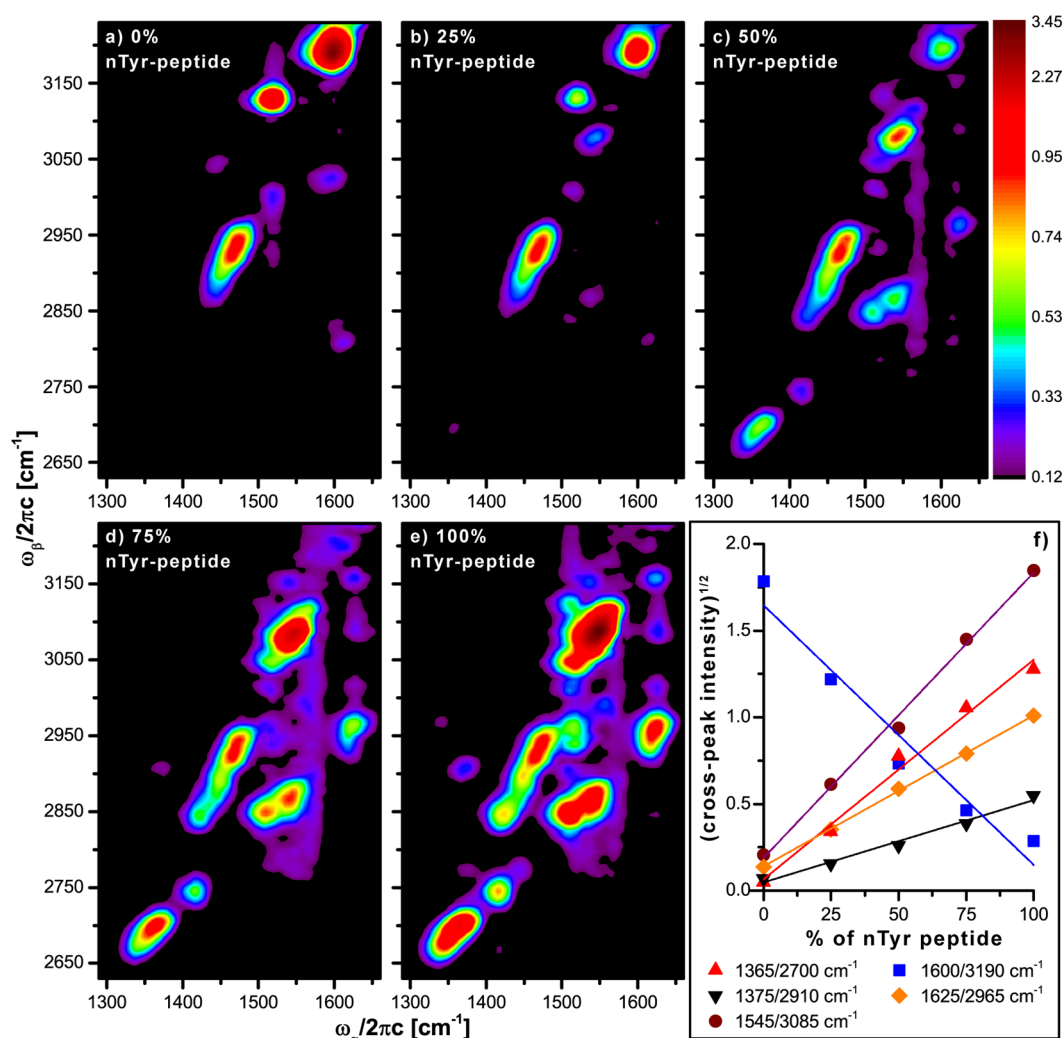


Figure 4. Experimental EVV 2DIR spectra for mixtures of the Tyr and nTyr heptamers at pH 9.1 containing (a) 0, (b) 25, (c) 50, (d) 75, and (e) 100% of the deprotonated nTyr peptide. The Tyr cross-peak intensities decrease and the nTyr cross-peak intensities increase with increasing percentage of nTyr in the peptide mixture. (f) Given that the signal depends on the square of the number of molecules, the square root of the normalized cross-peak intensity is plotted against the percentage of nTyr peptide. The linear regressions provide calibration curves from which the percentage of nTyr in a sample can be determined from the normalized cross-peak intensity.

deprotonated nTyr. From the data presented in Figure 4f and using the analysis described above for the pH 5.6 sample, we initially estimate a lower limit of 3% tyrosine nitration for the deprotonated state.

Spectra have also been measured for mixed-peptide samples containing 10 and 5% of the deprotonated nTyr peptide at pH 9.1 and are presented in Figure 5a and b, respectively. Because the relative intensities of the Tyr and nTyr peaks are so large at such low percentages of nTyr, the data have been plotted over a small frequency range so as to exclude the most intense Tyr peaks. In the 10% nTyr spectrum, the nTyr peak at 1545/3085 cm^{-1} (nTyr⁻⁸) is clearly visible, but in the 5% spectrum, this peak is barely discernible above the signal from neighboring features. The nTyr spectral signature is more clearly observed in the line profiles shown in Figure 5c for the 10 and 5% nTyr samples; these have been measured with the $\omega_{\alpha}/2\pi c$ frequency fixed at 1545 cm^{-1} on the center of the cross-peak, whereas the $\omega_{\beta}/2\pi c$ frequency is varied across the peak. The peaks centered at 3085 and 3132 cm^{-1} are assigned to nTyr and Tyr, respectively. The data presented in Figure 5c are the average of at least three line profiles, each obtained using longer data

acquisition times per point than for the spectra. Furthermore, a step size of 2 cm^{-1} has been used for the profile measurements compared to 5 cm^{-1} for the spectra, and a 5-point smoothing function has been applied. The consequence of using this alternative method is that the nTyr⁻⁸ peak at 3085 cm^{-1} is clearly discernible above the underlying signal in the line profiles for both the 10 and 5% samples.

The nTyr peak intensity values measured at 3085 cm^{-1} in the line profiles shown in Figure 5c were compared to the linear regression in Figure 4f for the 1545/3085 cm^{-1} peak (nTyr⁻⁸). This analysis yielded nTyr percentage values of 11 and 6%, which are in close agreement with the known values of 10 and 5% nTyr, respectively. On the basis of the low noise level observed for the line profiles in Figure 5c, and the clear separation observed between the profiles for the 5 and 0% samples, we estimate a lower detection limit of 1% for deprotonated nTyr, and we infer a lower detection limit of 4% for neutral nTyr.

An advantage of using EVV 2DIR spectroscopy is that it can also distinguish between the neutral and deprotonated states of nTyr. Therefore, this technique can potentially be used to

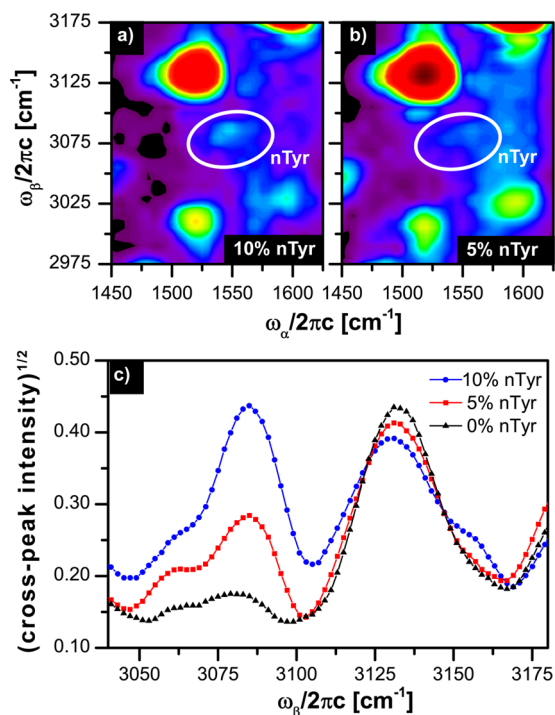


Figure 5. Experimental EVV 2DIR spectra for peptide samples at pH 9.1 in which (a) 10 and (b) 5% of the Tyr residues are nitrated. A weak nTyr⁻⁸ peak at 1545/3085 cm^{-1} is observed in both spectra and is indicated by a white circle. (c) Line profiles measured across EVV 2DIR spectral features using a fixed $\omega_a/2\pi c$ frequency value of 1545 cm^{-1} for 10, 5, and 0% nTyr samples at pH 9.1. The detection limit for tyrosine nitration can be determined by interpolation and is estimated to be 1%.

detect the level of tyrosine nitration in biological samples in their native states and to determine the relative abundances of the two protonation states, which will also provide an indication of the sample pH. Finally, potentially significant improvement in the sensitivity limit of EVV 2DIR can be had by introducing a resonant Raman probe step using a UV wavelength that is resonant with an electronic excitation level in nTyr such that it selectively enhances the signal level from nTyr residues. This could increase the signal level by several orders of magnitude, which is anticipated to improve the detection limit for nTyr to a value substantially lower than 1%.

3.4. Mass Spectrometry of Tyr/nTyr Peptide Mixtures.

For comparison with the EVV 2DIR quantification of tyrosine nitration, relative quantification was also performed by liquid chromatography-mass spectrometry (LC-MS). Small changes in the peptide structures, such as replacement of Tyr with nTyr, can result in significantly different signal intensities in LC-MS depending on a number of physicochemical properties of the peptides, the most important being their ionization efficiencies. To allow for this, accurately prepared solutions of pure peptides were used to generate a correction factor for relative quantitative analysis of the mixtures. Signals for the 1+ and 2+ ions, and their respective adducts with sodium, were observed in the spectra, and the sum of the areas of the peaks in the extracted ion chromatograms (XICs) for all of these species was used in the quantification (Figure 6). The nTyr peptide signal was observed to be approximately 2.61-fold more intense than that of the Tyr-containing peptide, and this factor was used to correct for the relative intensities in the LC-MS profile of the peptide mixtures.

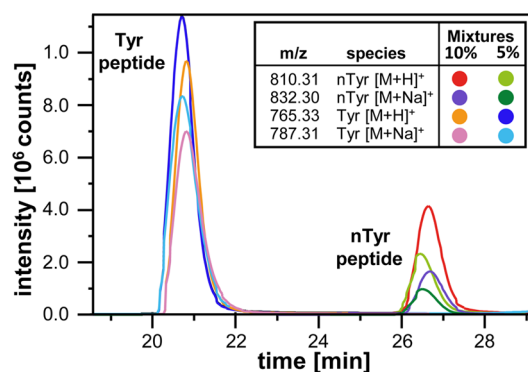


Figure 6. Section of the extracted ion chromatograms for peptide mixtures containing 5 and 10% of the nTyr peptide. The Tyr-containing peptide elutes at 20.8 min and nTyr-containing peptide at 26.6 min. Peaks appearing at the same retention times are for the 1+ charge states of the protonated and sodiated adducts. The relative abundance of nTyr appears to be more than 10% due to the more efficient ionization of the nTyr-containing peptide.

Quantitative mass spectrometric analysis of the peptide mixtures based on extracted ion chromatograms gave ratios of 5.4 and 12.1% for the 5 and 10% mixtures, respectively. This is in reasonably good agreement with the values of 6 and 11%, respectively, obtained using EVV 2DIR spectroscopy. It is interesting to note that the values obtained using both LC-MS and EVV 2DIR are consistently higher than the “known” nTyr values of 5 and 10%, which may indicate that these particular peptide samples have a higher proportion of nTyr than anticipated. This is highly plausible because of difficulties in handling small volumes of nTyr peptide solutions that are required for preparing low-percentage nTyr samples.

4. CONCLUSIONS

We have demonstrated the ability of EVV 2DIR spectroscopy to identify tyrosine nitration in short peptide models and to differentiate between the neutral and deprotonated states of nTyr. Detailed characterization of the experimental spectra has been carried out using the results of quantum chemistry calculations and by comparison with simulated EVV 2DIR spectra. Spectra have been measured for mixed-peptide samples containing levels of tyrosine nitration down to 5%. Following optimization of our data collection procedure, we were able to deduce nitration levels of 6 and 11% for selected mixed-peptide samples, which is in close agreement with the known values of 5 and 10%, respectively. Mass spectrometry was used to independently verify the level of nitration, yielding values of 5.4 and 12.1%. Interpolation of our EVV 2DIR line profiles indicates that the detection limits for tyrosine nitration are 1 and 4% for the deprotonated and neutral states of nTyr, respectively. We propose that this technique has the potential to detect low levels of protein tyrosine nitration in biological samples following the introduction of a resonant Raman probe step to increase the detection sensitivity. In summary, EVV 2DIR spectroscopy is able to provide detailed spectroscopic information on peptide side-chain modifications and to detect tyrosine nitration levels down to 1%.

■ ASSOCIATED CONTENT

Supporting Information

Results obtained from quantum chemistry calculations are provided for side-chain analogues of Tyr, neutral nTyr, and

deprotonated nTyr. The calculated normal modes are assigned, and the vibrational frequencies are compared with experimental values determined from EVV 2DIR spectra of model peptides (Tables S1, S2, and S3). This material is available free of charge via the Internet at <http://pubs.acs.org>.

AUTHOR INFORMATION

Corresponding Author

*E-mail: d.klug@imperial.ac.uk. Phone: (+44) 207 594 5806. Fax: (+44) 207 594 5880.

Present Address

[§]R.G.: Department of Chemistry, University College London, 20 Gordon St., London WC1H 0AJ, U.K.

Notes

The authors declare no competing financial interest.

ACKNOWLEDGMENTS

This work has been supported by the Proxomics project funded by the U.K. Engineering and Physical Sciences Research Council (EPSRC) (Grant EP/I017887/1). L.R.V. acknowledges additional support from the U.K. EPSRC through a doctoral training grant studentship (EP/J500239/1).

REFERENCES

- (1) Dalle-Donne, I.; Rossi, R.; Colombo, R.; Giustarini, D.; Milzani, A. Biomarkers of Oxidative Damage in Human Disease. *Clin. Chem.* **2006**, *52*, 601–623.
- (2) Halliwell, B.; Zhao, K.; Whiteman, M. Nitric Oxide and Peroxynitrite. The Ugly, the Uglier and the Not so Good: A Personal View of Recent Controversies. *Free Radical Res.* **1999**, *31*, 651–669.
- (3) Ischiropoulos, H. Protein Tyrosine Nitration—an Update. *Arch. Biochem. Biophys.* **2009**, *484*, 117–121.
- (4) Radi, R. Nitric Oxide, Oxidants, and Protein Tyrosine Nitration. *Proc. Natl. Acad. Sci. U.S.A.* **2004**, *101*, 4003–4008.
- (5) Abello, N.; Kerstjens, H. A.; Postma, D. S.; Bischoff, R. Protein Tyrosine Nitration: Selectivity, Physicochemical and Biological Consequences, Denitration, and Proteomics Methods for the Identification of Tyrosine-Nitrated Proteins. *J. Proteome Res.* **2009**, *8*, 3222–3238.
- (6) Radi, R. Protein Tyrosine Nitration: Biochemical Mechanisms and Structural Basis of Functional Effects. *Acc. Chem. Res.* **2013**, *46*, 550–559.
- (7) Gow, A. J.; Duran, D.; Malcolm, S.; Ischiropoulos, H. Effects of Peroxynitrite-Induced Protein Modifications on Tyrosine Phosphorylation and Degradation. *FEBS Lett.* **1996**, *385*, 63–66.
- (8) Horiguchi, T.; Uryu, K.; Giasson, B. I.; Ischiropoulos, H.; Lightfoot, R.; Bellmann, C.; Richter-Landsberg, C.; Lee, V. M.-Y.; Trojanowski, J. Q. Nitration of Tau Protein Is Linked to Neurodegeneration in Tauopathies. *Am. J. Pathol.* **2003**, *163*, 1021–1031.
- (9) Giasson, B. I.; Duda, J. E.; Murray, I. V.; Chen, Q.; Souza, J. M.; Hurtig, H. I.; Ischiropoulos, H.; Trojanowski, J. Q.; Lee, V. M. Oxidative Damage Linked to Neurodegeneration by Selective Alpha-Synuclein Nitration in Synucleinopathy Lesions. *Science* **2000**, *290*, 985–989.
- (10) Kummer, M. P.; Hermes, M.; Delekarte, A.; Hammerschmidt, T.; Kumar, S.; Terwel, D.; Walter, J.; Pape, H.-C.; König, S.; Roeber, S.; et al. Nitration of Tyrosine 10 Critically Enhances Amyloid B Aggregation and Plaque Formation. *Neuron* **2011**, *71*, 833–844.
- (11) Peluffo, G.; Radi, R. Biochemistry of Protein Tyrosine Nitration in Cardiovascular Pathology. *Cardiovasc. Res.* **2007**, *75*, 291–302.
- (12) Turko, I. V.; Murad, F. Protein Nitration in Cardiovascular Diseases. *Pharmacol. Rev.* **2002**, *54*, 619–634.
- (13) Yakovlev, V. A.; Bayden, A. S.; Graves, P. R.; Kellogg, G. E.; Mikkelsen, R. B. Nitration of the Tumor Suppressor Protein p53 at Tyrosine 327 Promotes p53 Oligomerization and Activation. *Biochemistry* **2010**, *49*, 5331–5339.
- (14) Ghesquière, B.; Colaert, N.; Helsens, K.; Dejager, L.; Vanhaute, C.; Verleysen, K.; Kas, K.; Timmerman, E.; Goethals, M.; Libert, C.; et al. In Vitro and in Vivo Protein-Bound Tyrosine Nitration Characterized by Diagonal Chromatography. *Mol. Cell. Proteomics* **2009**, *8*, 2642–2652.
- (15) Abello, N.; Barroso, B.; Kerstjens, H. A.; Postma, D. S.; Bischoff, R. Chemical Labeling and Enrichment of Nitrotyrosine-Containing Peptides. *Talanta* **2010**, *80*, 1503–1512.
- (16) Wright, J. C. Multiresonant Coherent Multidimensional Spectroscopy. *Annu. Rev. Phys. Chem.* **2011**, *62*, 209–230.
- (17) Zhao, W.; Wright, J. Doubly Vibrationally Enhanced Four Wave Mixing: The Optical Analog to 2D NMR. *Phys. Rev. Lett.* **2000**, *84*, 1411–1414.
- (18) Fournier, F.; Guo, R.; Gardner, E. M.; Donaldson, P. M.; Loeffeld, C.; Gould, I. R.; Willison, K. R.; Klug, D. R. Biological and Biomedical Applications of Two-Dimensional Vibrational Spectroscopy: Proteomics, Imaging, and Structural Analysis. *Acc. Chem. Res.* **2009**, *42*, 1322–1331.
- (19) Zhang, D.; Xie, Y.; Mrozek, M. F.; Ortiz, C.; Davison, V. J.; Ben-Amotz, D. Raman Detection of Proteomic Analytes. *Anal. Chem.* **2003**, *75*, 5703–5709.
- (20) Donaldson, P. M.; Guo, R.; Fournier, F.; Gardner, E. M.; Barter, L. M. C.; Barnett, C. J.; Gould, I. R.; Klug, D. R.; Palmer, D. J.; Willison, K. R. Direct Identification and Decongestion of Fermi Resonances by Control of Pulse Time Ordering in Two-Dimensional IR Spectroscopy. *J. Chem. Phys.* **2007**, *127*, 114513.
- (21) Guo, R.; Fournier, F.; Donaldson, P. M.; Gardner, E. M.; Gould, I. R.; Klug, D. R. Detection of Complex Formation and Determination of Intermolecular Geometry through Electrical Anharmonic Coupling of Molecular Vibrations Using Electron-Vibration-Vibration Two-Dimensional Infrared Spectroscopy. *Phys. Chem. Chem. Phys.* **2009**, *11*, 8417–8421.
- (22) Kwak, K.; Cha, S.; Cho, M.; Wright, J. C. Vibrational Interactions of Acetonitrile: Doubly Vibrationally Resonant IR–IR–visible Four-Wave-Mixing Spectroscopy. *J. Chem. Phys.* **2002**, *117*, 5675.
- (23) De Filippis, V.; Frasson, R.; Fontana, A. 3-Nitrotyrosine as a Spectroscopic Probe for Investigating Protein Protein Interactions. *Protein Sci.* **2006**, *15*, 976–986.
- (24) Donaldson, P. M.; Guo, R.; Fournier, F.; Gardner, E. M.; Gould, I. R.; Klug, D. R. Decongestion of Methylene Spectra in Biological and Non-Biological Systems Using Picosecond 2DIR Spectroscopy Measuring Electron-Vibration–Vibration Coupling. *Chem. Phys.* **2008**, *350*, 201–211.
- (25) Fournier, F.; Gardner, E. M.; Guo, R.; Donaldson, P. M.; Barter, L. M. C.; Palmer, D. J.; Barnett, C. J.; Willison, K. R.; Gould, I. R.; Klug, D. R. Optical Fingerprinting of Peptides Using Two-Dimensional Infrared Spectroscopy: Proof of Principle. *Anal. Biochem.* **2008**, *374*, 358–365.
- (26) Fournier, F.; Gardner, E. M.; Kedra, D. A.; Donaldson, P. M.; Guo, R.; Butcher, S. A.; Gould, I. R.; Willison, K. R.; Klug, D. R. Protein Identification and Quantification by Two-Dimensional Infrared Spectroscopy: Implications for an All-Optical Proteomic Platform. *Proc. Natl. Acad. Sci. U.S.A.* **2008**, *105*, 15352–15357.
- (27) Barth, A.; Zscherp, C. What Vibrations Tell about Proteins. *Q. Rev. Biophys.* **2002**, *35*, 369–430.
- (28) Lessing, J.; Roy, S.; Reppert, M.; Baer, M.; Marx, D.; Jansen, T. L. C.; Knoester, J.; Tokmakoff, A. Identifying Residual Structure in Intrinsically Disordered Systems: A 2D IR Spectroscopic Study of the GVGXPGVG Peptide. *J. Am. Chem. Soc.* **2012**, *134*, 5032–5035.
- (29) Varsányi, G. *Assignments for Vibrational Spectra of 700 Benzene Derivatives*; Institute of Physics Publishing: London, 1974; p 614.
- (30) Wilson, E. B. The Normal Modes and Frequencies of Vibration of the Regular Plane Hexagon Model of the Benzene Molecule. *Phys. Rev.* **1934**, *45*, 706–714.